2021

A Hybrid Simulation Model to Predict the Steady-State Thermal Profile of Hermetic Reciprocating Compressors

Fernando A. Aardoom
POLO Research Laboratories for Emerging Technologies in Cooling and Thermophysics, Federal University of Santa Catarina, Florianopolis, SC, Brazil

Victor H. P. Rosa
victor.rosa@polo.ufsc.br

Cesar J. Deschamps

A Hybrid Simulation Model to Predict the Steady-State Thermal Profile of Hermetic Reciprocating Compressors

Fernando A. AARDOOM, Victor H. P. ROSA, Cesar J. DESCHAMPS*

[1]POLO Research Labs, Federal University of Santa Catarina
Florianopolis, SC, Brazil
fernando.aardoom@polo.ufsc.br, victor.rosa@polo.ufsc.br, deschamps@polo.ufsc.br

* Corresponding Author

ABSTRACT

Numerical simulation models are paramount to design compressors that follow reliability and efficiency requirements. This paper presents a simulation model to predict the steady-state thermal profile of hermetic reciprocating compressors. A finite element method is used to compute the temperature distribution of the solid components and the fluid in the suction and discharge lines, whereas a lumped-parameter formulation is used to evaluate the internal environment temperature and the gas temperature at the end of the compression cycle. The heat transfer between the gas and the solid components is predicted using imposed convective heat transfer coefficients; some of which are estimated using heat transfer correlations, and others calibrated using experimental data and a genetic optimization algorithm. The numerical results were validated by comparisons with experimental data for different operating conditions and rotation speeds, showing that the model can be used to predict the compressor thermal profile in the entire application envelope. The low computational cost of the model enables its application to carry out sensitivity analysis and to assess thermal management alternatives to improve the compressor reliability or thermodynamic performance.

1. INTRODUCTION

Suction gas superheating can significantly reduce the thermodynamic performance of hermetic reciprocating compressors used in refrigeration systems, as it reduces the refrigerant gas density at the inlet of the compression chamber and therefore the mass flow rate supplied by the compressor. The three main heat sources of superheating in reciprocating compressors are: the electric motor, which generates heat due to electrical losses; the mechanism bearing, which generates heat due to mechanical friction; and the refrigerant gas at the discharge line of the compressor, which leaves the compression chamber at high pressure and temperature. In addition to the effect on gas superheating, high operating temperatures can affect the integrity and reliability of key components, such as the electric motor windings. Therefore, the prediction of the temperature distribution in hermetic reciprocating compressors and the assessment of thermal management solutions are important aspects of compressor design.

The temperature profile of hermetic reciprocating compressors can be measured directly by thermocouple wires, for example. Measurements are very accurate, but they are costly and time consuming, which can make it impractical to assess thermal management alternatives to improve the compressor performance. Numerical simulation tools, therefore, can be applied as an alternative to experimental activities. As they are cheaper and less time consuming, and if they are accurate enough, they can be very useful to perform such analyses.

Several numerical methodologies have been developed to predict the temperature distribution of reciprocating compressors. Sim et al. (2000) and Dutra and Deschamps (2015), for example, applied lumped-parameter formulations to predict the steady-state thermal profile of reciprocating compressors. In their methodology, the equations of conservation of mass and of energy are applied to several control volumes that represent the gas chambers in the compressor, which are linked through equivalent thermal conductances obtained from experimental calibration or correlations available in literature. These models can be applied for a low-cost estimation of the thermal behavior of reciprocating compressors, but are not accurate enough to capture the changes that may arise from subtle geometric changes.

More complex computational tools to predict the thermal behavior of hermetic reciprocating compressors have been presented by Chikurde et al. (2002) and Birari et al. (2006). In these distributed-parameter models based on the finite volume method, velocity, pressure and temperature profiles are predicted for both solid and fluid domains. The main difference between them is that the model by Chikurde et al. (2002) couples the fluid at the suction and discharge lines considering a polytropic process, whereas the model by Birari et al. (2006) solves the fluid flow in the compression chamber using a dynamic mesh. Oliveira et al. (2017) also applied a finite volume method to predict the temperature distribution and the fluid flow for a linear compressor, whose operation is based on a linear motor and a spring. Despite of their accuracy, distributed-parameter models present high computational cost and difficulty to model the lubricating oil flow inside the compressor, which directly impacts its thermal behavior.

Hybrid simulation models such as those presented by Ribas (2007), Schreiner et al. (2009) and Sanvezzo Jr. and Deschamps (2012) combine lumped-parameter and distributed-parameter formulations, coupling them iteratively. In the hybrid approach, the thermal interactions between the different control volumes are predicted using equivalent thermal conductances, while the heat conduction through the solid components is calculated using a differential model. The model described by Ribas (2007) applies global heat transfer coefficients obtained from experimental calibration and calculates temperatures for the fluid and solid domains using energy balances. This simulation provides the boundary conditions (temperatures and heat transfer coefficients) required by the distributed-parameter model. Once solved, the heat conduction model provides the heat fluxes through the solid components, which return to the lumped-parameter formulation to adjust the thermal profile. In order to increase the flexibility of this kind of approach, Sanvezzo Jr. and Deschamps (2012) proposed the calculation of the global heat transfer coefficients using heat transfer correlations from the literature and considered the effect of the lubricant oil flow inside the compressor shell. In order to quantify this effect, Sanvezzo Jr. and Deschamps (2012) considered that 80% of the lubricant oil mass flow rate is directed to the shell surface, while the rest of it flows to the crankcase region.

Comparing the studies available in literature concerned with numerical simulation models for the thermal management of hermetic reciprocating compressors, it can be noted that the lumped-parameter formulations are accurate to predict the thermal interactions between the refrigerant gas and solid components through the application of energy balances and thermal conductances, making them particularly useful when low computational costs are required at initial design steps. However, lumped models present relevant limitations as they are not capable of predicting the heat conduction and the temperature stratification at the solid components and gas chambers. On the other hand, distributed-parameter models can accurately simulate the fluid flow through the fluid chambers and the heat conduction through the solid components, but they present a high computational cost, reducing their applicability when a large design space must be considered to improve compressor efficiency.

One of the advantages of a hybrid approach is that the thermal interactions between fluid and solid domains can be modelled without solving the fluid flow, so that a low simulation time is achieved when compared to distributed-parameter models that solve the temperature, velocity and pressure fields for the fluid domains. Additionally, the heat conduction through the solid components, which is not solved in lumped-parameter formulations, can be efficiently predicted using a finite element method, since the mesh requirements are less strict compared to models based on a finite volume method. The hybrid models found in literature, however, do not simulate the temperature stratification at the refrigerant gas, applying lumped models for the gas.

This paper presents a hybrid simulation model to predict the steady-state thermal profile of the solid components and the refrigerant gas of hermetic reciprocating compressors. The model couples distributed-parameter models to predict the temperature stratification on the solid components and the refrigerant gas with lumped-parameter formulations to calculate the internal environment temperature and the temperature rise in the compression cycle. Due to its low computational cost, the model can be applied to assess thermal management solutions and to perform sensitivity analysis, therefore aiding the design of hermetic reciprocating compressors.

2. METHODOLOGY

In the model presented in this paper, the compressor CAD model is used to describe the solid domain. The fluid domains are represented by tubes that are drawn across the chambers in the suction and discharge lines. The following hypotheses were made regarding the refrigerant gas flow: unidimensional, incompressible, inviscid and in steady-state regime. Therefore, for the two fluid domains (the suction and discharge lines), as the cross-section of the tubes is

constant, the velocity distribution is trivial and the numerical solution used to obtain the temperature distribution along the domain. For that, fixed mass flow rate and temperature-dependent specific heat coefficients must be assigned.

The heat conduction in the solid components is modelled by the thermal energy equation and the Fourier's Law, and is solved numerically by a finite element method. Considering a steady-state operation and homogeneous and isotropic materials, the heat conduction equation is

$$k\nabla^2 T + \dot{q} = 0, \tag{1}$$

where k is the thermal conductivity, ∇^2 is the Laplace operator, T is the temperature, and $\dot{q}$ is the volumetric heat generation.

The thermal interactions between the refrigerant gas and the solid components is predicted by the application of a coupled solution of the heat transfer problem on the fluid-solid interfaces. Figure 1 shows a representation of the different methods that are coupled to predict the thermal interactions in the compressor. The pipes shown in black represent the fluid domain, which is discretized in elements that interact with the surface elements of the solid domain based on the proximity between them. As a result of the thermal interactions between the fluid and solid elements, the temperature along the fluid line vary, and this stratification affects the local heat transfer with the solid components.

In order to calculate the heat transfer between the external surfaces of the solid components and the internal environment, and between the internal environment and the compressor shell, convective heat transfer coefficients and an internal environment temperature are defined. Since the internal environment temperature is not known at the beginning of the simulation, it is calculated iteratively based on a lumped formulation and a thermal circuit that represents the heat transfer between the internal components and the shell, as shown in Figure 2.

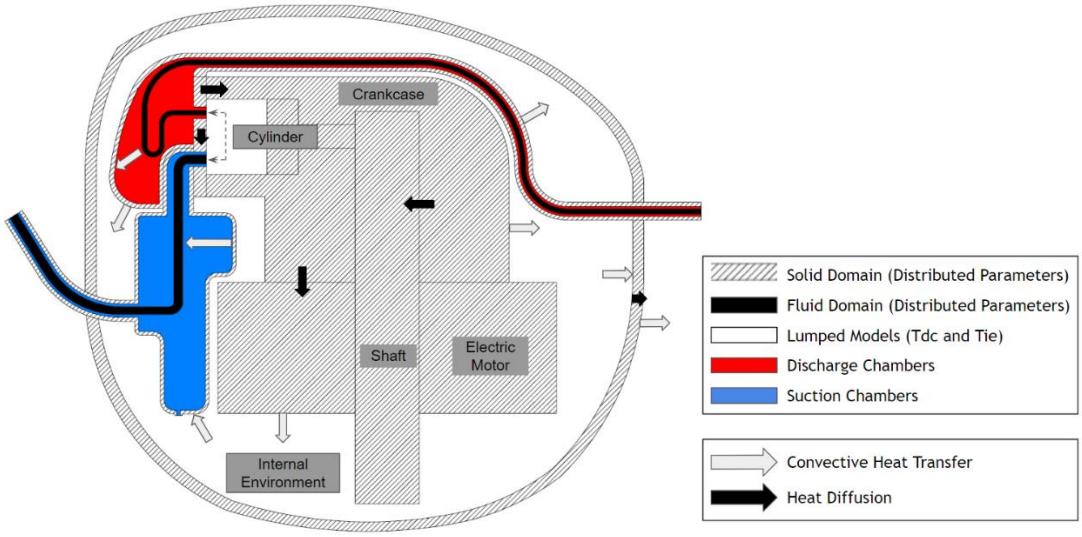

Figure 1: Methods that are coupled to predict the thermal interactions in the compressor.

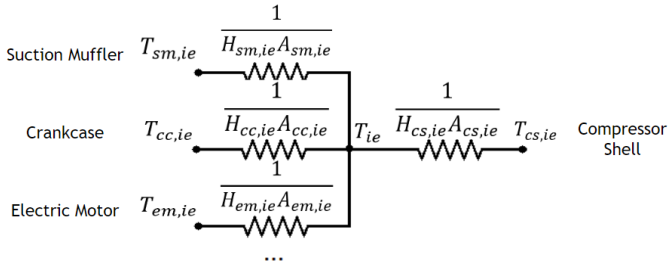

Figure 2: Thermal circuit between the internal components and the compressor shell.

Considering a steady-state operation, the sum of the heat exchanged between the internal components and the internal environment must be transferred to the internal surface of the compressor shell before leaving the compressor to the external ambient. Therefore, the average temperatures at the surface of each solid component ($T_{i,ie}$) can be related to the internal environment temperature (T_{ie}) and to the average temperature at the internal surface of the compressor shell ($T_{cs,ie}$) by performing an energy balance. After algebraic manipulation, an explicit equation for T_{ie} is written:

$$T_{ie} = \frac{\sum H_{i,ie} A_{i,ie} T_{i,ie} + H_{cs,ie} A_{cs,ie} T_{cs,ie}}{\sum H_{i,ie} A_{i,ie} + H_{cs,ie} A_{cs,ie}} \tag{3}$$

where the convective heat transfer coefficients between each internal component and the internal environment ($H_{i,ie}$) and the convective heat transfer coefficient between the internal environment and the shell internal surface ($H_{cs,ie}$) are adjusted using experimental data. The surface areas of the components ($A_{i,ie}$) and the shell internal surface area ($A_{cs,ie}$) are obtained from the CAD model. The surface-average temperatures $T_{i,ie}$ and $T_{cs,ie}$ are obtained from the distributed-parameter model.

The heat transfer between the compressor external surface and the external ambient is computed using values of temperature and heat transfer coefficients. The external environment temperature must be prescribed, while an equivalent heat transfer coefficient (H_{eq}) that considers convection and radiation is calculated as

$$H_{eq} = H_{ee} + \left[\sigma\epsilon\left(T_{cs,ee}^4 - T_{ee}^4\right)\right]\left(T_{cs,ee} - T_{ee}\right)^{-1} \tag{4}$$

where σ is the Stefan-Boltzmann constant, ϵ is the emissivity of the compressor external surfaces, $T_{cs,ee}$ is the average temperature on the external surface of the shell and T_{ee} is the external ambient temperature. The convective heat transfer coefficient between the compressor shell and the external environment is calculated using the correlation proposed by Yovanovich (1987) for arbitrarily-shaped immersed bodies, in which the Nusselt number is given by

$$Nu_L = 3.47 + 0.51 Ra_L^{1/4} \tag{5}$$

where Ra_L is the Rayleigh number with the square root of the exposed surface area as characteristic length. For the internal flow in the discharge tube and in the inlet and outlet pipes, the heat transfer coefficients are calculated using the Dittus-Boelter correlation for turbulent flow.

The two fluid lines that represent the refrigerant gas in the suction and discharge lines of the compressor require an inlet temperature as a boundary condition. The inlet temperature of the suction line must be prescribed as a boundary condition for the problem, whereas the inlet temperature of the discharge line is calculated based on the gas temperature at the end of the suction line. The refrigerant gas enthalpy at the end of the compression process, h_{dc}, is calculated using the first law of thermodynamics

$$h_{dc} = h_{sc} + \frac{1}{\dot{m}}\left(\dot{W}_{th} - \dot{Q}_{cc}\right), \tag{6}$$

where h_{sc} is the refrigerant gas specific enthalpy at the inlet of the compression chamber, $\dot{m}$ is the mass flow rate, and $\dot{W}_{th}$ is the thermodynamic power. For the results presented in this paper, the compression process is considered adiabatic, so that $\dot{Q}_{cc}$ is set to zero.

The refrigerant gas mass flow rate attributed to the fluid domain must be imposed as a boundary condition. Additionally, the electric power must be known in order to compute the heat generated due to electrical and mechanical losses and the thermodynamic power delivered to the refrigerant gas in the compression process. In order to define these values, the following three basic options are available: i) imposing the mass flow rate and the electric power based on the compressor datasheet or experimental data; ii) predicting the mass flow rate and the electric power using the semi-empirical model described by Li (2012); iii) imposing a volumetric flow rate and the electric power and predicting the mass flow rate based on the refrigerant gas density at the compression chamber inlet. For the second option, the semi-empirical model coefficients must be adjusted using the compressor datasheet or experimental data.

For the third option, a reference volumetric flow rate ($\dot{V}_{ref}$) can be obtained by simulating the model with reference input parameters and based on the following equation:

$$\dot{m} = \rho_{sc}\dot{V}_{ref} \tag{7}$$

The numerical solution is obtained by solving the distributed-parameter model using a commercial finite element solver. The calculation of the internal environment temperature and the temperature of the refrigerant gas at the end of the compression process is based on lumped models implemented in programming scripts that are coupled internally to the finite element solver. The first step in the solution procedure consists on the definition of input parameters and initial estimates for the two variables that depend on the lumped formulations: the discharge temperature (T_{dc}) and the internal environment temperature (T_{ie}). Once $\dot{m}$ is attributed for the fluid domain, T_{dc} is set as a boundary condition at the first node of the discharge line and T_{ie} is set as condition to calculate the heat transfer between the internal components and the internal environment. Then, the distributed-parameter model is solved, hence updating the suction temperature (T_{sc}), the average temperatures at the components surfaces ($T_{i.ie}$) and the average temperature on the compressor shell's internal surface ($T_{cs,ie}$). These updated variables are used to calculate new values for T_{dc} and T_{ie} using the lumped-parameter formulations. Additionally, if the volumetric flow rate is defined, the mass flow rate is updated using the new gas density at the inlet of the compression chamber. A flowchart of the numerical procedure is shown in Figure 3.

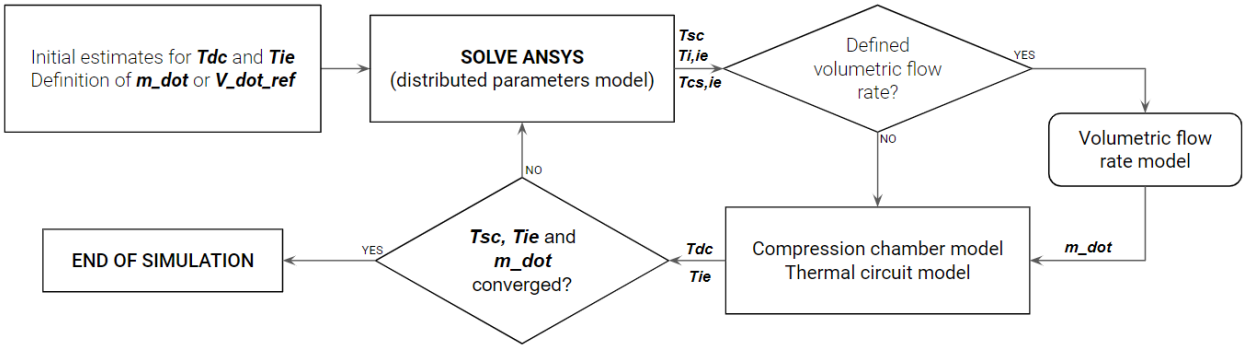

Figure 3: Flowchart of the solution procedure.

3. RESULTS

The experimental results presented hereafter were obtained for a low-capacity reciprocating compressor with a displacement of 9.04 cm³ operating with R600a in a hot-cycle calorimeter bench (Dutra and Deschamps, 2009). The numerical results were obtained using the compressor CAD model assuming constant electrical and mechanical efficiencies of 86% (except for the sensitivity analysis of the electrical efficiency) and 90%, respectively. Additionally, the compressor's external surface emissivity was defined at 0.9. Values for the temperature of the gas at the compressor inlet and for the external environment temperature were defined based on the experimental tests.

3.1. Model calibration and validation

The model calibration is performed by simulating the compressor with prescribed electric power and mass flow rate taken from experiments and comparing the predicted temperature with measured data at 8 locations. Then, 7 heat transfer coefficients and a multiplication factor for external heat transfer coefficient are adjusted by using the 8 selected temperatures as targets of an optimization routine using a genetic algorithm. The operating condition used for the calibration consists of an evaporating temperature of -20°C and a condensing temperature of 45°C, with the compressor operating at 4000 rpm. The parameters that were calibrated in the numerical model, their respective constraints and final results are shown in Table 1.

When applying the model for other conditions, the adjusted heat transfer coefficients in the suction and discharge chambers (H_{sl} and H_{dl}) are updated based on the functional dependence of the Nusselt number with the mass flow rate given by the Dittus-Boelter correlation, i.e.

$$H_{sl} = \left(\frac{\dot{m}}{\dot{m}_{calib}}\right)^{\frac{4}{5}} H_{sl,calib}; \quad H_{dl} = \left(\frac{\dot{m}}{\dot{m}_{calib}}\right)^{\frac{4}{5}} H_{dl,calib} \tag{8}$$

The model validation was performed by analyzing numerical predictions for 9 operating conditions that consist in combinations of the evaporating temperatures of -30°C, -20°C and -10°C and condensing temperatures of 35°C, 45°C and 55°C. In Table 2, the 8 temperatures that were considered as targets for the calibration procedure are shown for the calibration condition and for two other extreme conditions (with a high mass flow rate, *Validation 1*; and with a low mass flow rate, *Validation 2*). The numerical results were obtained with the model using experimental results for the mass flow rate and electric power. The calibration is considered adequate, since all the predicted temperatures are within ±1ºC of the measured data for the calibration condition. For both validation conditions, the cylinder temperature presented the highest deviations in relation to experimental results, reaching a maximum absolute value of 4.2°C in *Validation 2*, but most of the predicted temperatures are within ±2ºC of the experimental data.

Figure 4 shows a comparison between experimental and numerical results obtained with the numerical model by imposing measured values for the mass flow rate and the electric power for the 9 operating conditions, all for a rotational speed of 4000 rpm. As can be seen, the numerical results are in good agreement with the experimental data in magnitude and trend. The largest deviations in relation to experimental results are observed for the cylinder temperature (maximum deviation around 4°C), followed by the electric motor temperature. The smallest differences between experimental and numerical results are observed for the internal environment temperature (T_{ie}) and for the temperatures of the refrigerant gas at the outlet of the suction muffler and at the discharge chamber.

Figure 5 shows a comparison between numerical results obtained with imposed experimental values for $\dot{m}$ and $\dot{W}$ and numerical results obtained with $\dot{m}$ and $\dot{W}$ predicted using the semi-empirical model described by Li (2012). By noting that the temperature predictions using both methods are similar, it is shown that the semi-empirical model can be used to predict the compressor thermal profile for conditions without measured mass flow rate and electric power. For these predictions, the model by Li (2012) has been implemented and calibrated with measurements of $\dot{m}$ and $\dot{W}$.

Figure 6 presents a comparison between experimental and numerical results obtained by imposing measured $\dot{m}$ and $\dot{W}$ at a rotational speed of 2000 rpm. Larger deviations compared to experimental data were obtained for the evaporating temperature of -30°C, especially for the discharge temperature (maximum around 5°C) and the cylinder temperature (maximum around 7°C). An interesting fact is that these deviations get smaller when the evaporating temperature increases, showing that the model becomes more accurate when the mass flow rate gets closer to the calibration condition (the model was calibrated at 4000 rpm). Additionally, Figure 6 presents values of T_{dc} obtained with the model without correcting the heat transfer coefficients in the suction and discharge chambers (Eqs. (8) and (9)), showing that the correction improves the accuracy of the model.

Table 1: Calibrated parameters and results of the calibration procedure.

Parameter	Bounds	Result
Hee_{factor} (-)	[1, 20]	7.4
$H_{sm,ie}$ (W m^{-2} K^{-1})	[50, 150]	115
$H_{dt,ie}$ (W m^{-2} K^{-1})	[50, 150]	40
$H_{cc,ie}$ (W m^{-2} K^{-1})	[50, 150]	140
$H_{em,ie}$ (W m^{-2} K^{-1})	[50, 150]	65
$H_{cs,ie}$ (W m^{-2} K^{-1})	[50, 300]	250
$H_{sl,calib}$ (W m^{-2} K^{-1})	[100, 400]	250
$H_{dl,calib}$ (W m^{-2} K^{-1})	[100, 800]	720

Table 2: Experimental and numerical results for the targets of the optimization procedure.

	Calibration (-20°C/45°C)			Validation 1 (-10°C/35°C)			Validation 2 (-30°C/55°C)		
Results	**Exp.**	**Num.**	**Dif.**	**Exp.**	**Num.**	**Dif.**	**Exp.**	**Num.**	**Dif.**
T_{mo} (°C)	45.9	45.1	-0.8	35.3	34.9	-0.4	44.9	44.4	-0.5
T_{dc} (°C)	93.1	93.0	-0.1	75.7	77.0	1.3	94.8	96.2	1.4
T_{em} (°C)	60.0	59.7	-0.3	50.9	52.3	1.4	57.2	54.1	-3.1
T_{cw} (°C)	66.8	66.8	0.0	55.6	57.9	2.3	65.9	61.7	-4.2
T_{sm} (°C)	50.9	51.2	0.3	40.8	42.2	1.4	50.5	48.0	-2.5
T_{ie} (°C)	54.6	55.4	0.8	47.0	47.6	0.6	50.7	50.6	-0.1
T_{dl} (°C)	66.3	65.4	-0.9	58.3	58.2	-0.1	58.6	58.1	-0.5
T_{cs} (°C)	52.9	52.5	-0.4	45.8	44.9	-0.9	49.1	47.8	-1.3

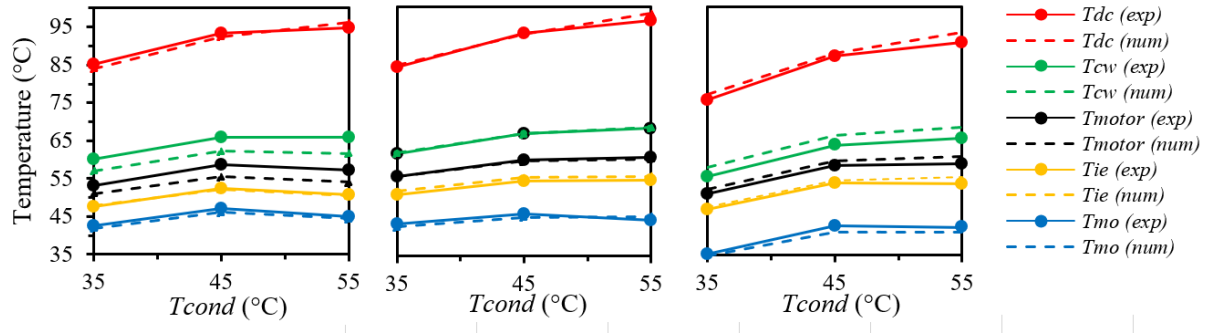

(a) *Tevap* = -30ºC (b) *Tevap* = -20ºC (c) *Tevap* = -10ºC

Figure 4: Comparison between experimental data (*exp*) and numerical predictions (*num*) using experimental data for $\dot{m}$ and $\dot{W}$ for the compressor operating at 4000 rpm.

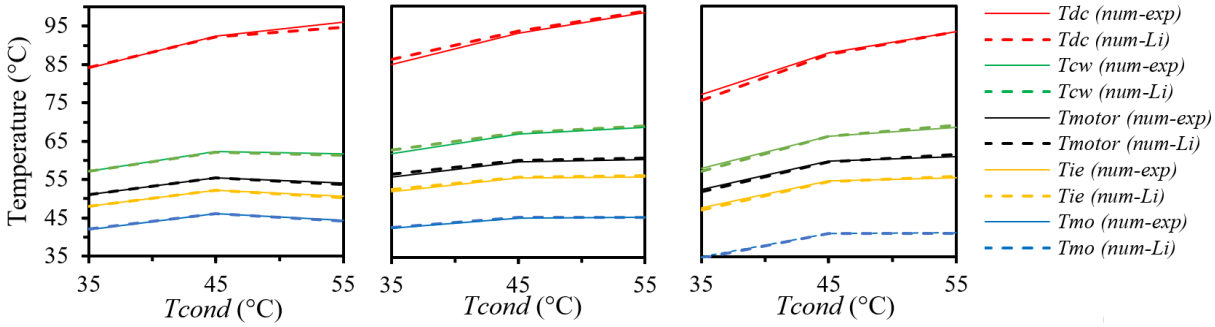

(a) *Tevap* = -30ºC (b) *Tevap* = -20ºC (c) *Tevap* = -10ºC

Figure 5: Comparison between numerical predictions using measured $\dot{m}$ and $\dot{W}$ (*num-exp*) with numerical predictions with $\dot{m}$ and $\dot{W}$ predicted with the model by Li (2012) (*num-Li*) for the compressor operating at 4000 rpm.

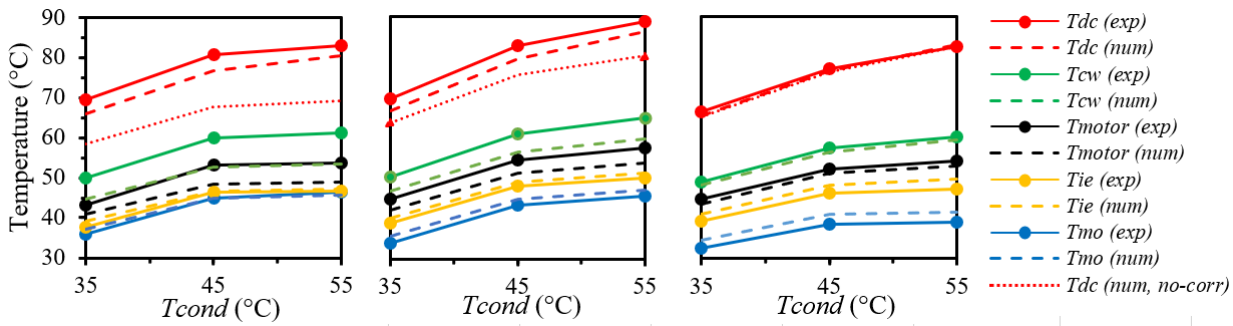

(a) *Tevap* = -30ºC (b) *Tevap* = -20ºC (c) *Tevap* = -10ºC

Figure 6: Comparison between measured data and numerical predictions for the compressor operating at 2000 rpm. The effect of updating H_{sl} and H_{dl} according to the mass flow rate for the prediction of T_{dc} is highlighted by comparing *"Tdc (num)*" with "*Tdc (num, no-corr)*".

3.2. Temperature contours

The refrigerant gas exchanges heat with the inlet pipe, the suction muffler, and the orifice in the valve plate before entering the compression chamber. As these components receive heat from the compressor internal environment and other components, superheating takes place at the suction line. Figure 7a presents the temperature distribution of the refrigerant gas at the suction line of the compressor for the calibration condition, showing an increase of approximately 13°C due to a heat transfer of approximately 16 W to the gas in the suction line. As a result of the compression process, the refrigerant gas leaves the compression chamber at 116°C and loses approximately 71 W of heat to the valve plate, the discharge chamber, the discharge muffler, the discharge pipe, and the outlet pipe, leaving the compressor at 65.4°C.

The temperature distribution of the refrigerant gas until it reaches the discharge tube is shown in Figure 7b. A large part of the gas cooling occurs right after it leaves the compression chamber, when it flows through the valve plate and the discharge chamber.

Figure 8a shows the internal thermal profile of the compressor for the calibration condition. The coldest regions are those in direct contact with the refrigerant gas at the suction line, whereas the hottest region comprises the discharge chamber. The maximum temperature observed for the electric motor (which is a critical component in terms of reliability) is approximately 60°C, which is considered acceptable. Figure 8b shows the thermal profile of the compressor shell for the calibration condition. This thermal profile is influenced by the contacts between the shell and the inlet and outlet pipes, which generate the regions with the extreme temperatures in blue and red.

3.3. Sensitivity analysis

A sensitivity analysis was performed to estimate the influence of the electric motor efficiency and the external ambient temperature on the thermodynamic performance and the reliability of the compressor. For this analysis, the model that considers a reference volumetric flow rate to predict the compressor mass flow rate was used, with the reference volumetric flow rate being computed by simulating the model for the calibration condition with an electrical efficiency of 86% and an external environment temperature of 33.2°C.

Figure 9a shows the change in temperatures of interest as a function of the motor electrical efficiency. The temperature of the electric motor varies with the greatest slope, indicating that the electrical efficiency is an important parameter in terms of reliability related to temperature. The influence of the electrical efficiency on the mass flow rate is also shown as a deviation from the reference mass flow rate for an electric efficiency of 86%. The effect of the ambient temperature on selected temperatures of interest and on the mass flow rate is shown in Figure 9b. The model predicts a reduction of approximately 0.7% in mass flow rate when the external environment temperature rises from 33.2°C to 38.2°C.

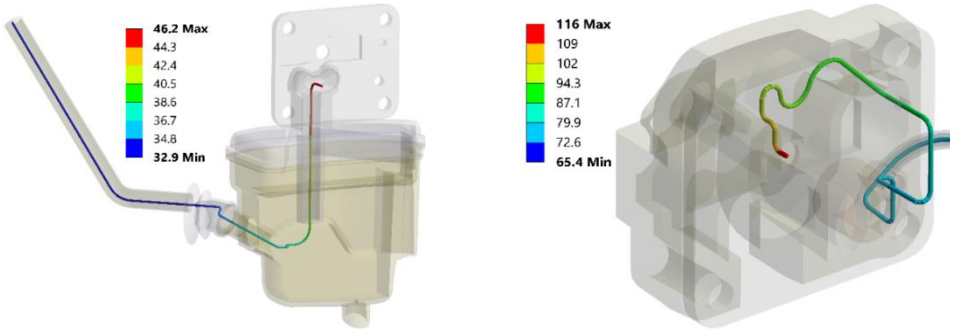

(a) (b)

Figure 7: Refrigerant gas temperature (a) throughout the suction line, and (b) at the beginning of the discharge line.

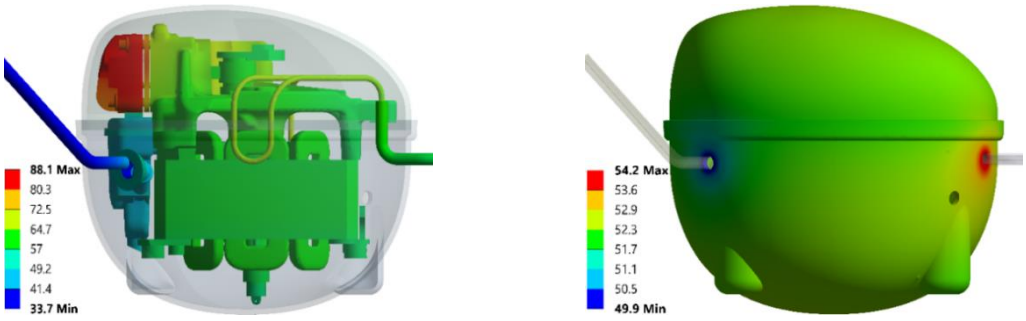

(a) (b)

Figure 8: Thermal profile of (a) the internal components and (b) the compressor shell.

In order to determine which is the main source of superheating and therefore reduction of volumetric efficiency, four simulations for the calibration condition were performed with different modifications in the compressor: i) with a perfectly insulated discharge line; ii) without mechanical losses; iii) without electrical losses; iv) with the valve plate's thermal conductivity divided by 100. Table 3 presents the results of these simulations, showing that the main source of superheating in the suction line is the gas in the discharge line. Insulating the discharge line reduced the superheating by approximately 9°C, whereas the other modifications yielded smaller superheating reductions.

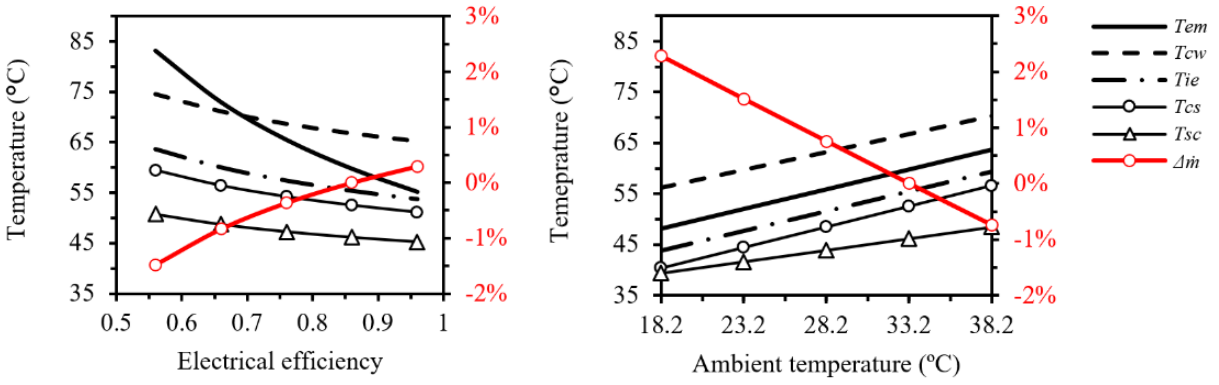

Figure 9: Impact of the (a) electrical efficiency and the (b) ambient temperature on temperatures and mass flow rate.

Table 3: Suction temperature and heat flow rates from/to the gas in the suction and discharge lines.

Condition	ΔT_{sc} (°C)	Heat flow rate from the gas in discharge line (W)	Heat flow rate to the gas in suction line (W)
Baseline	0.0	70.7	15.6
Insulated discharge line	-9.1	0.0	5.0
Without mechanical losses	-1.2	72.3	14.2
Without electrical losses	-1.3	71.8	14.1
Valve plate with lower thermal conductivity	-0.9	69.4	14.5

4. CONCLUSIONS

A simulation model to compute the thermal profile of hermetic reciprocating compressors was presented. The model applies a finite element method to solve the tridimensional heat conduction in the solid components of the compressor and the fluid flow in its tubes and chambers. The solid is considered homogeneous, but interfaces between different materials are allowed, and the fluid flow is considered inviscid, incompressible and unidimensional. To compute the convective heat transfer between the fluid and the solid, convective heat transfer coefficients were adjusted with an optimization algorithm and experimental data taken in a hot-cycle test rig. Additionally, the temperature distribution given by the finite element method is coupled to a lumped-parameter formulation for the fluid temperature in the internal environment and at the compression chamber outlet. To assess the model accuracy, its predictions for both solid surfaces and fluid regions were compared to thermocouple measurements at 9 operating conditions and 2 different rotational speeds, showing that the predictions are within 2°C for most of the measured data. Besides its accuracy, the distributed-parameter nature of the finite element method allows the visualization of the temperature profile inside the compressor, which can be used to understand the heat path in the compressor and improve its design.

NOMENCLATURE

Symbols

A	Area	(m^2)
ϵ	Emissivity	
h	Specific enthalpy	(J kg^{-1})
H	Convective heat transfer coeff.	(W m^{-2} K^{-1})
k	Thermal conductivity	(W m^{-1} K^{-1})
$\dot{m}$	Mass flow rate	(kg s^{-1})
Nu	Nusselt number	
$\dot{Q}$	Heat flux	(W)
$\dot{q}$	Volumetric heat generation	(W m^{-3})
Ra	Rayleigh number	
ρ	Density	(kg m^{-3})
σ	Stefan-Boltzmann constant	(W m^{-2} K^{-4})
T	Temperature	(ºC)
$\dot{V}$	Volumetric flow rate	(m^3 s^{-1})
$\dot{W}$	Power	(W)

Subscripts

calib	Related to the calibration condition
cc	Crankcase
cs,ee	External surface of the shell
cs,ie	Internal surface of the shell
cw	Cylinder wall
dc	Discharge chamber
dl	Discharge line
dt	Discharge tube
ee	External environment
em	Electric motor
eq	Equivalent
exp	Experimental
ie	Internal environment
mo	Suction muffler outlet
motor	Electric motor
num	Numerical
ref	Reference
sc	Suction chamber
sl	Suction line
sm	Suction muffler
th	Thermodynamic

REFERENCES

Birari, Y. V., Gosavi, S. S., & Jorwekar, P. P. (2006). Use of CFD in design and development of R404a reciprocating compressor. *Proc. Int. Compressor Eng. Conf. at Purdue,* West Lafayette, USA.

Chikurde, R. C., Longanathan, E., Dandekar, D. P., & Manivasagam, S. (2002). Thermal mapping of hermetically sealed compressors using computational fluid dynamics technique. *Proc. Int. Compressor Eng. Conf. at Purdue,* West Lafayette, USA.

Dutra, T., & Deschamps, C. J. (2015). A simulation approach for hermetic reciprocating compressors including electrical motor modeling. *Int. J. Refrig., 59.*

Li, W. (2012). Simplified steady-state modeling for hermetic compressors with focus on extrapolation. *Int. J. Refrigeration, 35, 1722-1733.*

Meyer, W. A., & Thompson, H. D. (1988). An analytical model of heat transfer to the suction gas in a low-side hermetic refrigeration compressor. *Proc. Int. Compressor Eng. Conf. at Purdue,* West Lafayette, USA.

Oliveira, M. J., Diniz, M. C., & Deschamps, C. J. (2017). Predicting the temperature distribution and suction gas superheating of an oil-free linear compressor. *Journal of Process Mechanical Engineering, 231(1), 47-56.*

Ribas Jr, F. A. (2007). Thermal analysis of reciprocating compressors. *Proc. Int. Conf. on Compressors and Their Systems,* London, UK.

Sanvezzo Jr, J., & Deschamps, C. J. (2012). A heat transfer model combining differential and integral formulations for thermal analysis of reciprocating compressors. *Proc. Int. Compressor Eng. Conf. at Purdue,* West Lafayette, USA.

Schreiner, J. E., Deschamps, C. J., Ribas Jr, F. A., Barbosa Jr, J. R., & Rosa, V. H. P. (2009). Thermal management of a commercial reciprocating compressor through numerical simulation. *Int. Conf. on Compressors and Coolants,* Castá Papiernicka, Slovakia.

Sim, Y. H., Youn, Y., & Min, M. K. (2000). A study on heat transfer and performance analysis of hermetic reciprocating compressors for refrigerators. *Proc. Int. Compressor Eng. Conf. at Purdue,* West Lafayette, USA.

ACKNOWLEDGEMENTS

The authors appreciate the support from Nidec-GA (Embraco) and EMBRAPII through Grant No. 202001416 (“Development of new technologies for refrigeration compressors" Project). Additional funding was provided by CAPES (Talents for Innovation Program - Grant No. 88887.194773/2018-00) and by the National Institutes of Science and Technology (INCT) Program (CNPq Grant No. 404023/2019-3; FAPESC Grant No. 2019TR0846).